This presentation participates in OSPP

Outstanding Student & PhD candidate Presentation contest

Impacts of atmospheric drivers on surface energy and mass components

as a function of the GrIS elevation and as dependent on key atmospheric circulation patterns

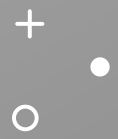

Tiago Silva[1], Jakob Abermann[1,2], Brice Noël[3], Sonika Shahi[1], Jorrit van der Schot[1], and Wolfgang Schöner[1]

[1]Institute for Geography and Regional Sciences, University of Graz, Austria

[2]Austrian Polar Research Institute, Vienna, Austria

[3]Institute for Marine and Atmospheric Research, Utrecht University, The Netherlands

Correspondent author: tiago.ferreira-da-silva@uni-graz.at

KARL-FRANZENS-UNIVERSITÄT GRAZ
UNIVERSITY OF GRAZ

Equilibrium line altitude (ELA)

$$SMB_{lat} = \sum_{Oct-Sep}^{daily} SMB_{lat_{daily}}$$

ELA/zone: 95th percentile of the ablation area altitude.

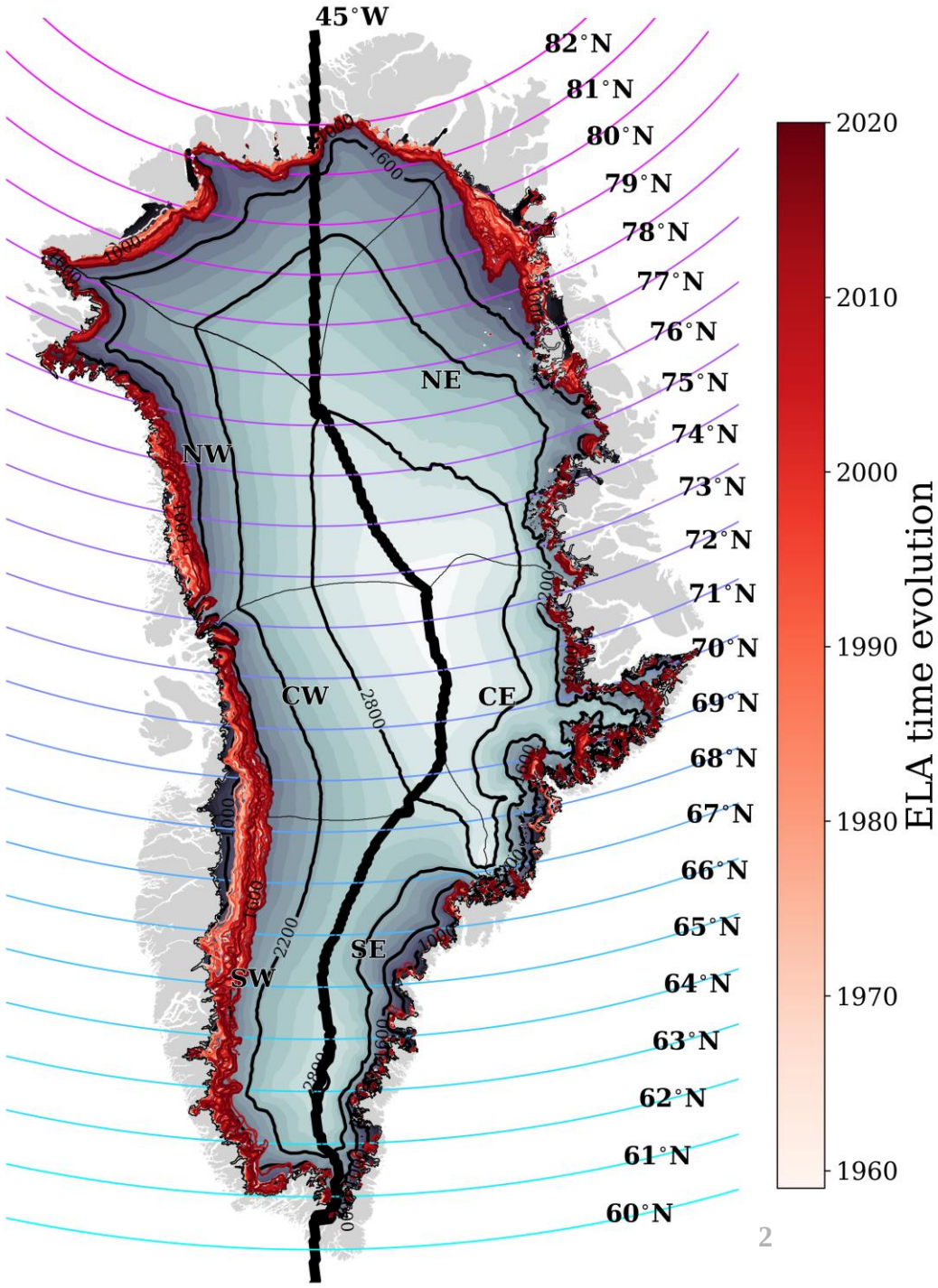

Figure 1 – Interannual variability of the Equilibrium Line Altitude from 1959 to 2020 derived from RACMO2.3p2 over the GrIS. The parallels used for latitudinal analysis of the annual ELA are displayed. The separation from West and East Greenland is indicated by the thick black line that goes along the GrIS crest until 76ºN and after follows the meridian 45ºW.

r_S(ELA, surface slope at ELA)

Rapid ELA migration on flatter surfaces.

2012 and 2019 the highest ELA.

High ELA variability over the SE.

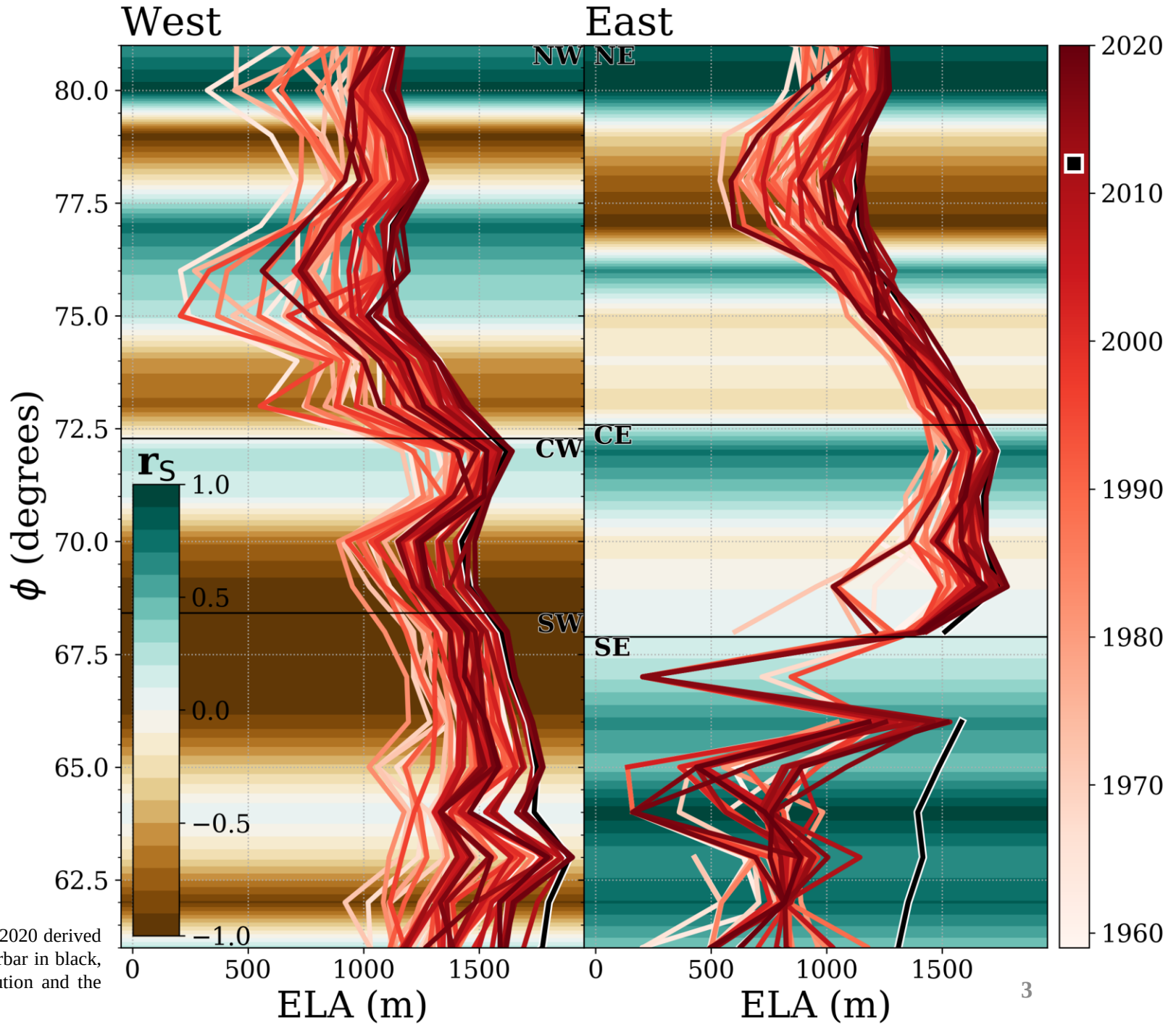

Figure 2 – Interannual variability of the ELA as a function of latitude from 1959 to 2020 derived from RACMO2.3p2 over the GrIS. 2012 is drawn and marked in the chart and colorbar in black, respectively. The Spearman correlation coefficient between the annual ELA evolution and the associated surface slope is color-coded.

$\mathbf{r_S}$(ELA, surface slope at ELA)

Repeatedly negative SMB_{lat}:

- between 65 and 70 degrees at Western GrIS;
- between 77 and 79 degrees at Eastern GrIS.

Larger SMB_{lat} losses in recent years than in 2012 at most latitudes.

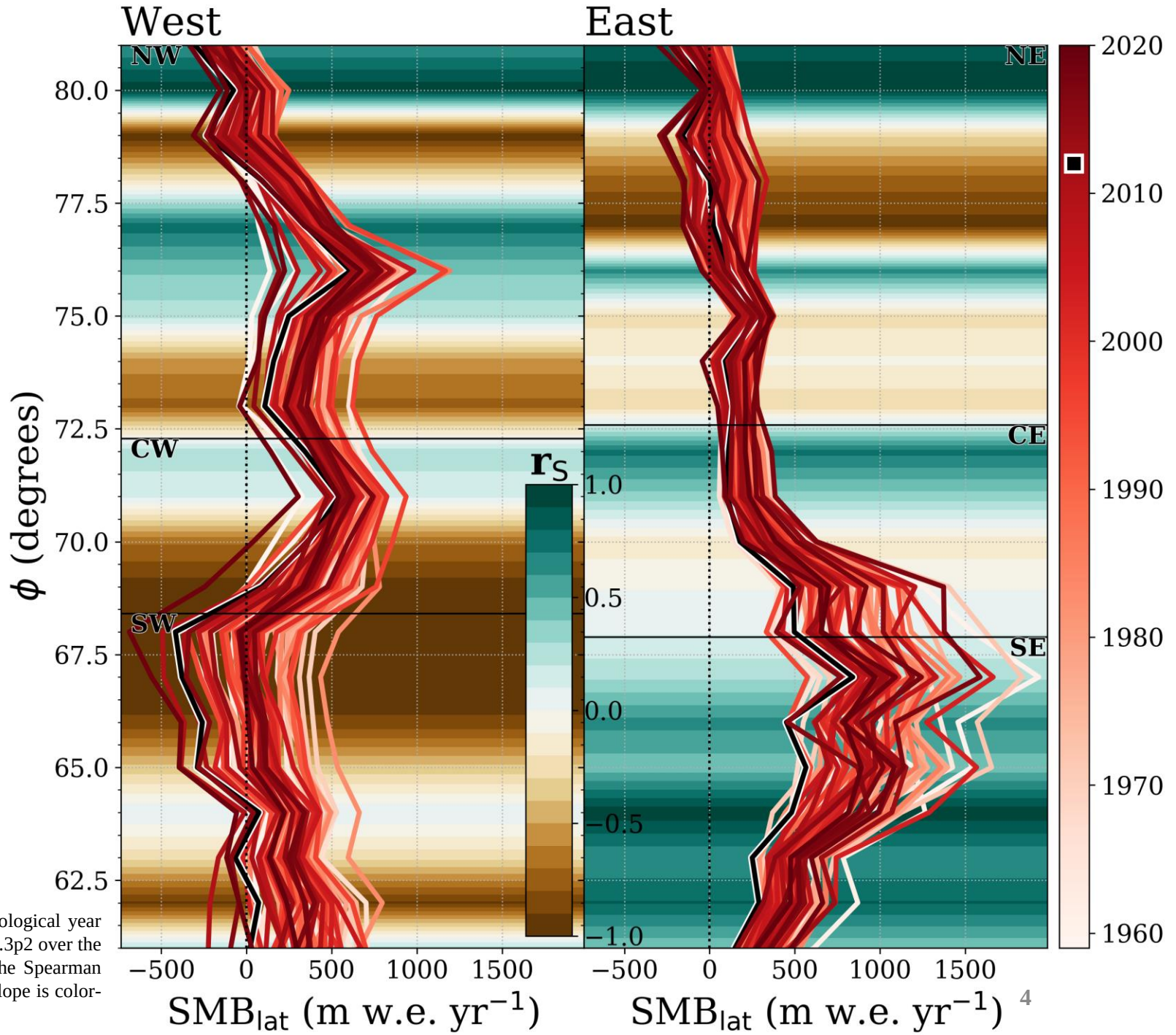

Figure 3 – Interannual variability of the SMB_{lat} (following the definition of the hydrological year indicated in Fig. 1) as a function of latitude from 1959 to 2020 derived from RACMO2.3p2 over the GrIS. 2012 is drawn and marked in the chart and colorbar in black, respectively. The Spearman correlation coefficient between the annual ELA evolution and the associated surface slope is color-coded.

North Atlantic influence over Greenland (**NAG**)

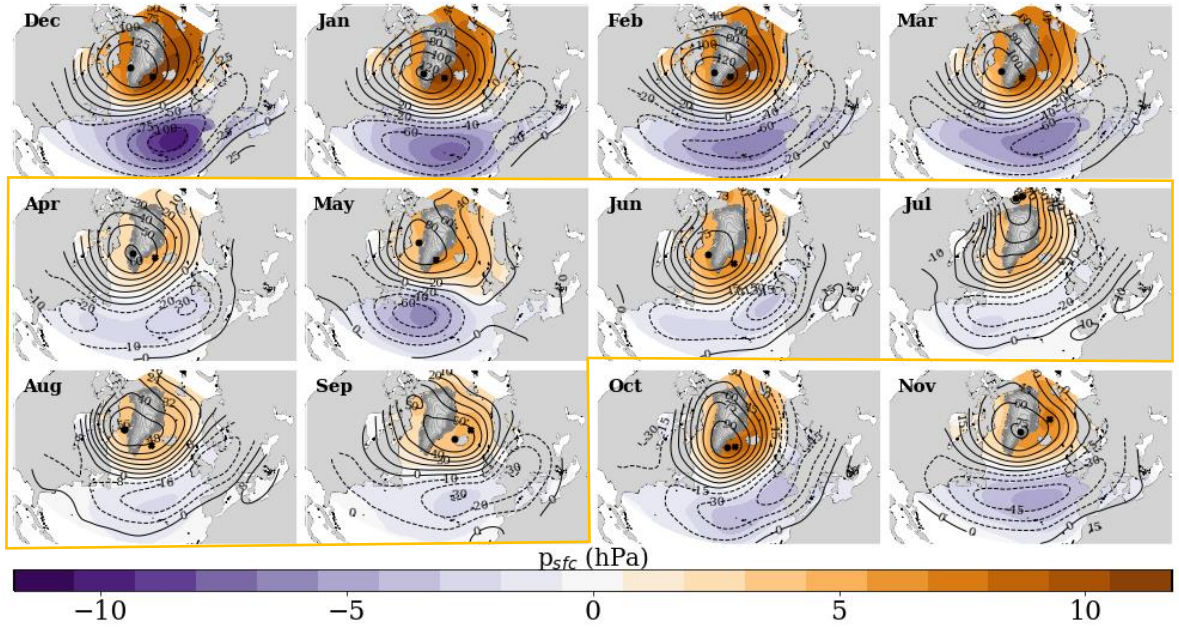

Figure 4 – Monthly +NAG at 500hPa geopotential height anomaly (positive: solid contour lines and negative: dashed contour lines) spaced in 10 m intervals, and surface pressure anomaly. Both anomalies with respect to climatology (1959-2000).

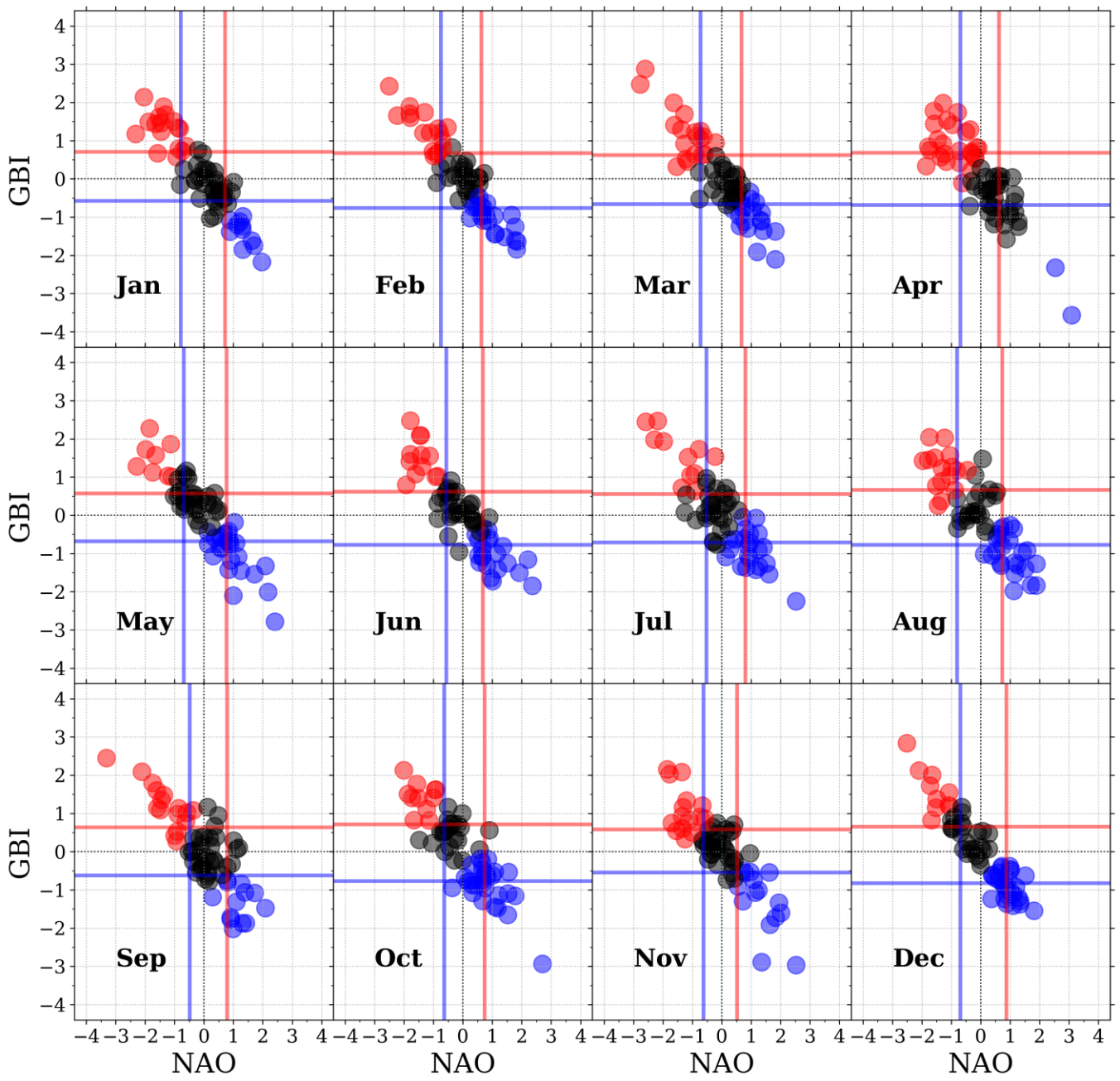

Figure 5 – Monthly NAG phases based on k-means clustering using the monthly NAO, GBI and IWV GrIS between 1959 and 2020: positive (red), neutral (black) and negative (blue) phase. Monthly 25th (blue line) and 75th (red line) percentiles for NAO and GBI are drawn as lines. Method thoroughly described in: Silva et al. (2022).

NAG evolution

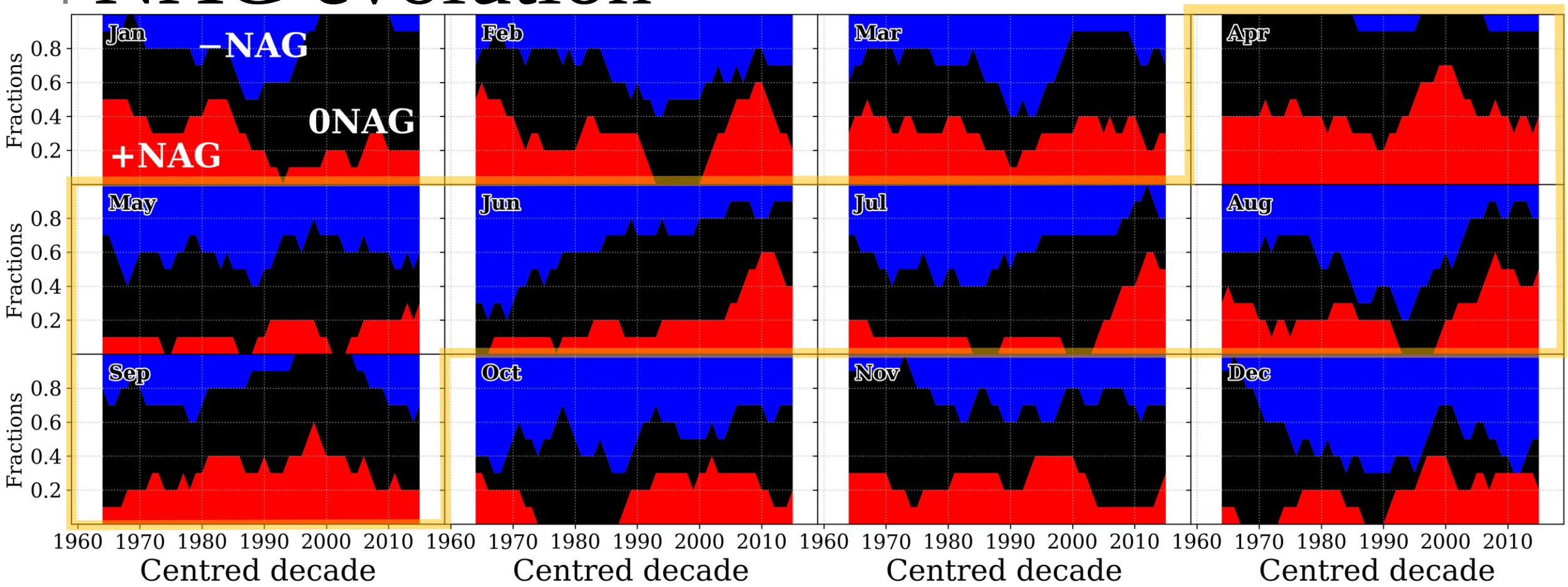

Figure 6 – 10-year running monthly NAG fractions. The warm season between April and September is highlighted. NAG is color-coded in accordance with Figure 4.

During the warm season, monthly +NAG has been occasionally since the 1990s more frequent than 0NAG and –NAG together.

Most frequent NAG in the warm season

Influence of the NAG on SMB_{lat} at West GrIS.

+NAG was once the most frequent NAG phase before 1991.

SMB_{lat} losses are regionally accentuated when +NAG is the most frequent NAG phase over the year (not shown).

For –NAG, the SMB_{lat} is regionally larger since 1991.

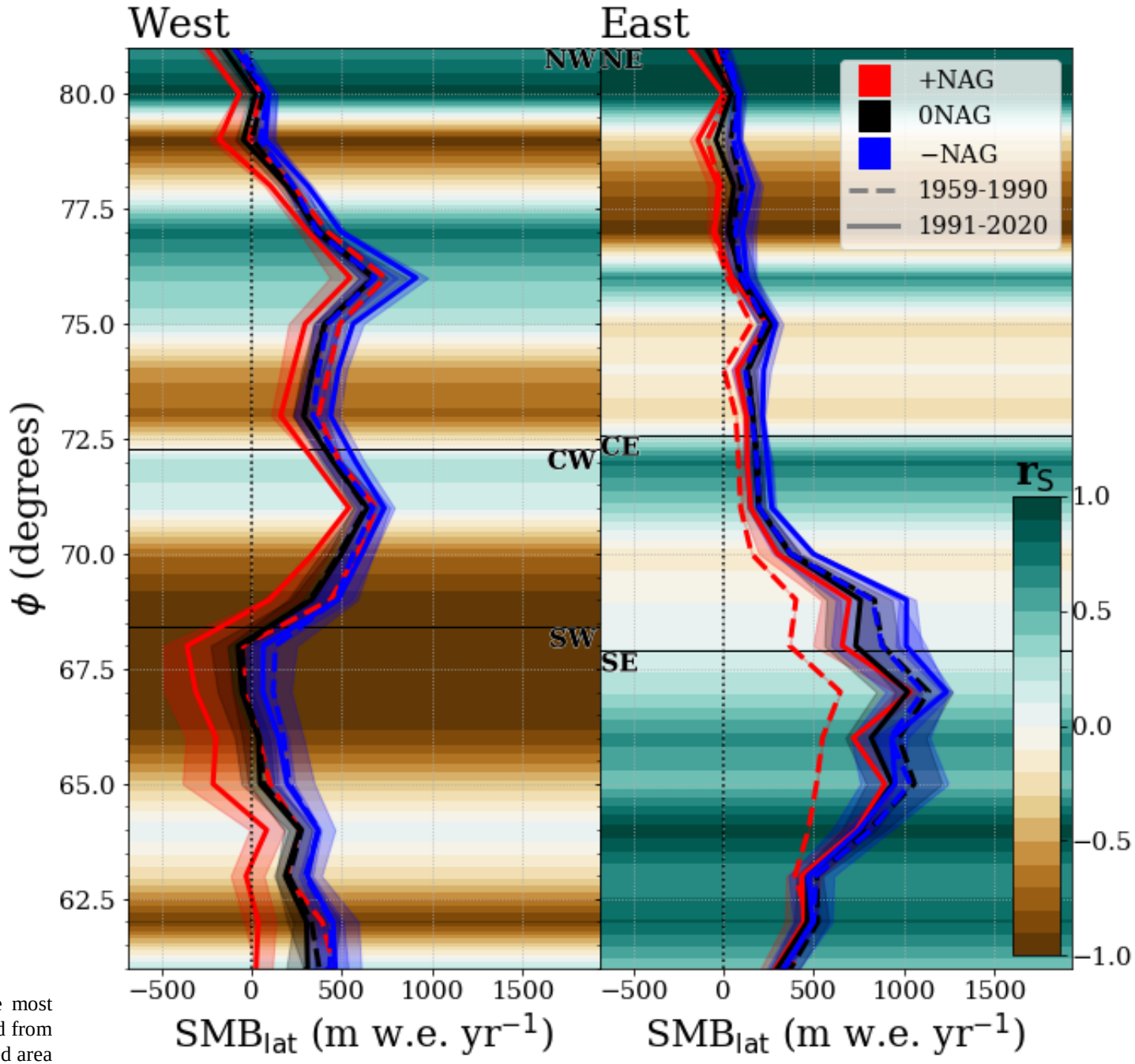

Figure 7 – Interannual variability of the SMB_{lat} as a function of latitude classified by the most frequent monthly NAG during the warm season (April - September) from 1959 to 2020 derived from RACMO2.3p2 over the GrIS. Years before (after) 1991 as dashed (continuous) line. The shaded area represents the IQR. The Spearman correlation coefficient between the annual ELA evolution and the associated surface slope is color-coded.

SEB components

Increasing SHF in early warm season.

Wide air temperature increase, particularly at high elevations.

Decreasing α in alignment with ΔM at West GrIS.

Turbulent fluxes contribution in the North to increasing ΔM.

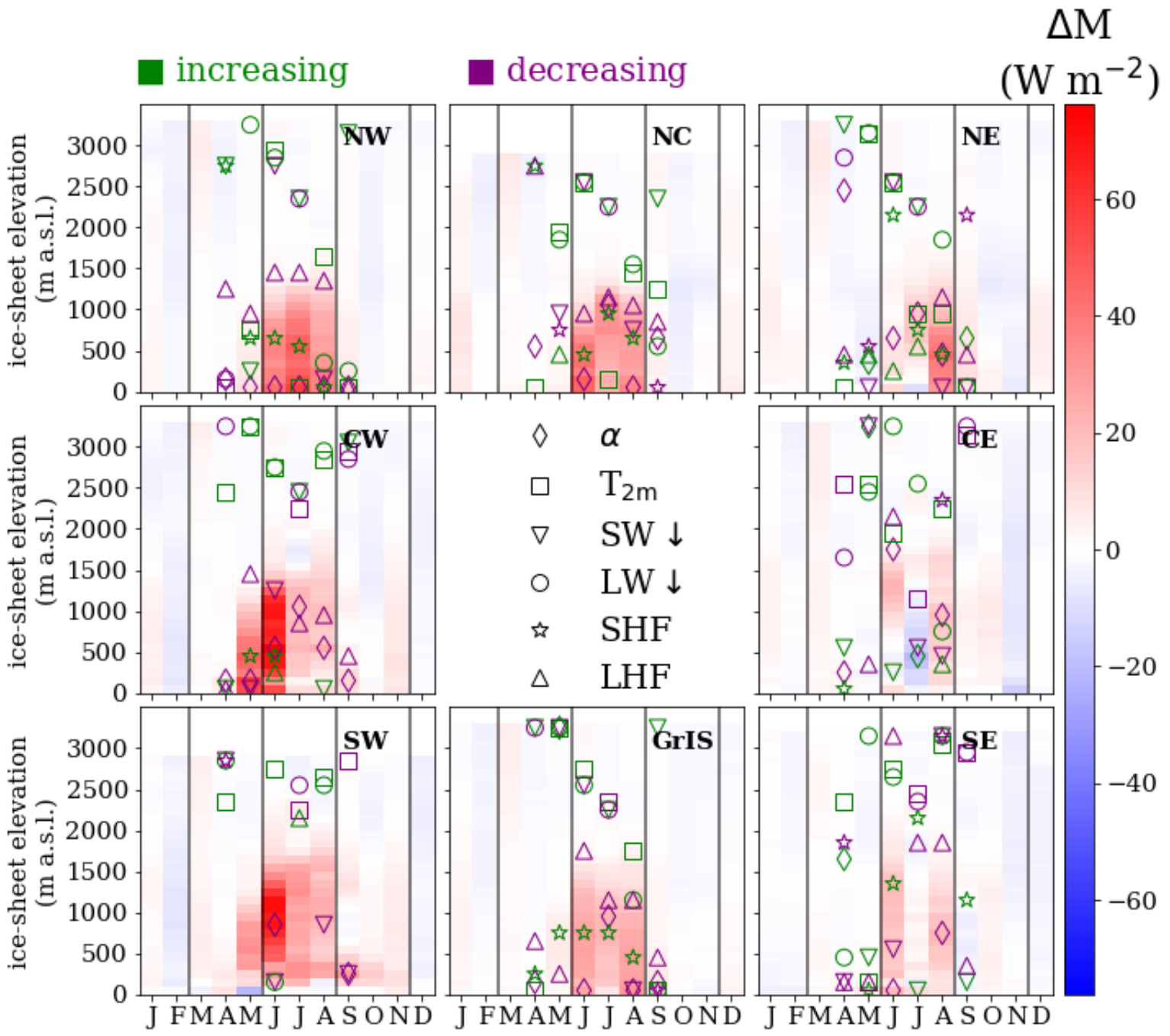

Figure 8 – Anomaly of the energy available to melt (ΔM) as a function of the ice-sheet elevation based on the composite difference (1991-2020 and 1959-1990) where +NAG was the most frequent NAG during the warm season from 1959 to 2020 derived from RACMO2.3p2. The greatest absolute change in albedo (α), two-meter air temperature (T_{2m}), incoming shortwave radiation (SW↓), incoming longwave radiation (LW ↓), sensible heat (SHF) and latent heat (LHF) flux is marked along the warm season when the statistical confidence is higher than 90% based on the Wilcoxon rank-sum statistic test for two unpaired samples.

SMB components

More precipitation in early warm season at the West GrIS.

More (less) winter (summer) precipitation at Southeast GrIS.

At high elevations, increased refreezing related to increased snowfall.

Continuous increasing in surface melt.

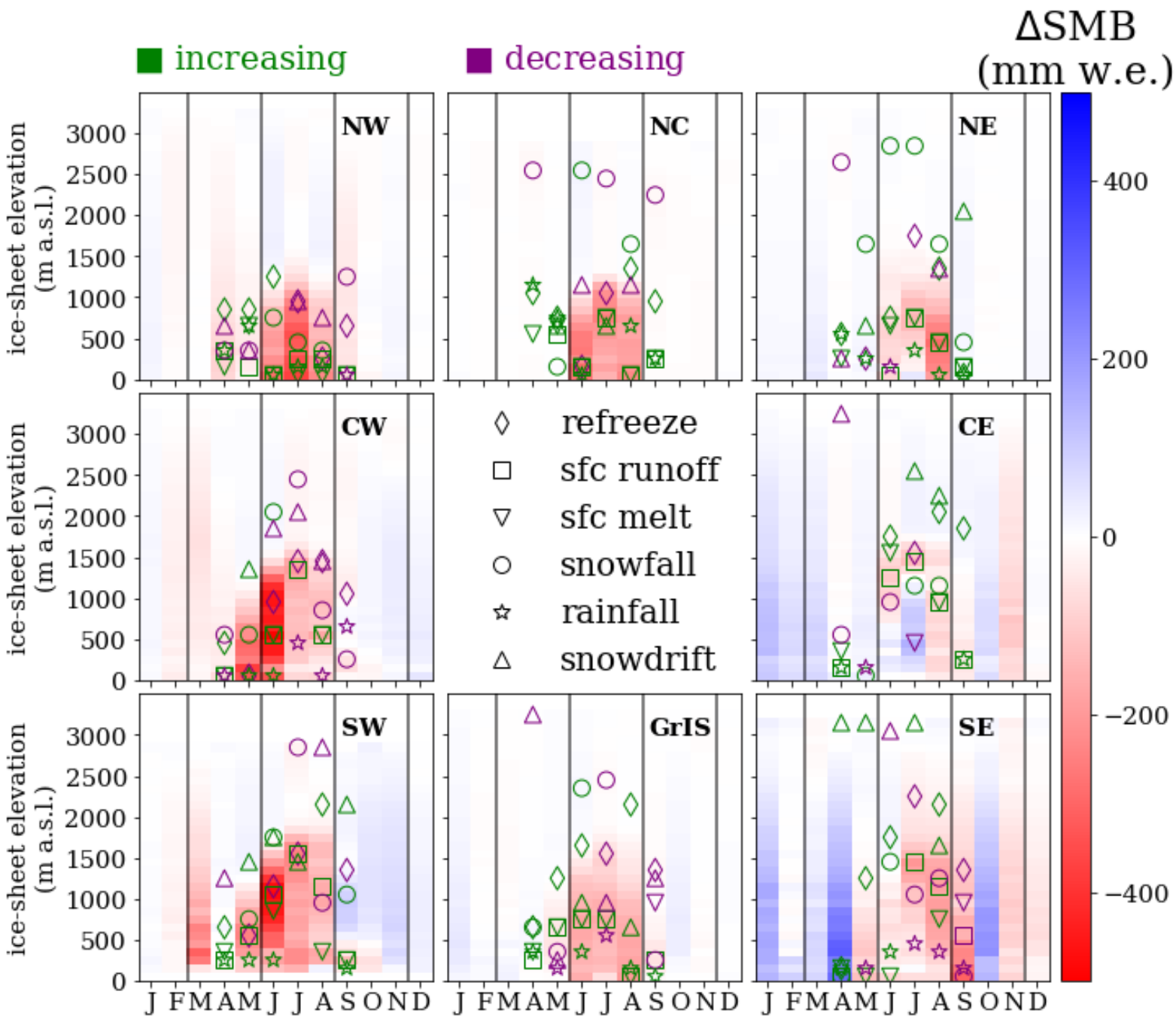

Figure 9 – Anomaly of the surface mass balance (ΔSMB) as a function of the ice-sheet elevation based on the composite difference (1991-2020 and 1959-1990) where +NAG was the most frequent NAG during the warm season from 1959 to 2020 derived from RACMO2.3p2. The greatest absolute change in albedo (α), two-meter air temperature (T_{2m}), incoming shortwave radiation (SW↓), incoming longwave radiation (LW ↓), sensible heat (SHF) and latent heat (LHF) flux is marked along the warm season when the statistical confidence is higher than 90% based on the Wilcoxon rank-sum statistic test for two unpaired samples.